Modelling Simul. Mater. Sci. Eng. **15** (2007) 275–284 doi:10.1088/0965-0393/15/3/006

An improved QM/MM approach for metals

Yi Liu, Gang Lu, Zhengzheng Chen and Nicholas Kioussis

Department of Physics and Astronomy, California State University Northridge, Northridge, CA 91330-8268, USA

E-mail: ganglu@csun.edu

Received 27 July 2006, in final form 7 February 2007
Published 15 March 2007
Online at stacks.iop.org/MSMSE/15/275

Abstract

We present an improved quantum mechanical (QM) and molecular mechanical (MM) coupling method for the study of metallic systems. The improved method is based on the earlier work of Choly *et al* (2005 *Phys. Rev.* B **71** 094101). In this approach, quantum mechanical treatment is spatially confined to a small region, surrounded by a larger molecular mechanical region. This approach is particularly useful for systems where quantum mechanical interactions in a small region, such as lattice defects or chemical impurities, can affect the macroscopic properties of a material. We discuss how the coupling across the different scales can be accomplished efficiently and accurately for metals. The method is tested by performing a multiscale simulation of bulk aluminium (Al) where the coupling errors can be easily analysed. We then apply the method to study the core structure and Peierls stress of an edge dislocation in Al.

(Some figures in this article are in colour only in the electronic version)

1. Introduction

The challenge in computational materials science and engineering is that real materials usually exhibit phenomena on one scale which require a very accurate and computationally expensive description and phenomena on another scale for which a coarser description is satisfactory and, in fact, necessary to avoid prohibitively large computations. It is the hope that multiscale modelling approaches may be the answer to such a challenge, and they are by definition computational approaches that take advantage of the multiple scales present in a material and build unified descriptions by linking the models specialized at different scales.

Two categories of multiscale simulations can be envisioned, sequential, consisting of passing information across scales, and concurrent, consisting of seamless coupling of scales [1]. The majority of multiscale simulations that are currently in use are sequential and are effective in systems where the various scales are weakly coupled. An example of a sequential approach is the Peierls–Nabarro (PN) model which essentially establishes a connection between atomic and continuum length scales [1,2]. The information passed across the scales is the generalized stacking fault energy surface which can be determined accurately from the density functional

theory (DFT) calculations. In systems where the coupling across different length scales is strong, concurrent approaches are usually required. In contrast to sequential approaches, concurrent simulations are still relatively new and only a few models have been developed to date [3–19]. In a concurrent simulation, the system is often partitioned into domains characterized by different scales and physics. The challenge of any concurrent approach lies in establishing a high quality coupling between the regions which are treated by different computational methods. Notably, Choly *et al* have recently put forward a general concurrent method which couples DFT-based quantum mechanical simulations to classical atomistic simulations for metallic materials [9]. The efficiency and accuracy of this coupling scheme have been demonstrated in bulk and a screw dislocation in Al. More recently, a multiscale approach was developed that concurrently couples DFT calculations for electrons to the embedded-atom-method (EAM) [20] simulations for classical atoms and to the finite-element modelling for elastic continuum in a unified fashion [11]. The approach, referred to as QCDFT, is based on the formalism of Choly *et al* and the quasicontinuum method [3, 8] and has been applied to study an edge dislocation in Al in the absence and presence of hydrogen impurities [11]. Despite the apparent success of the concurrent approach of Choly *et al* , non-negligible errors nonetheless exist across the DFT/EAM boundary [9]. More specifically, when the interaction energy between the quantum and classical regions is determined from a classical simulation, the forces on the atoms are determined by DFT and EAM *cluster* calculations where the fictitious surface effects cannot be fully cancelled owing to the mismatch in DFT/EAM forces on the surface atoms. The surface effects obtained can introduce substantial errors on the position of the atoms at the domain boundary and degrade the coupling across the boundary.

It is the purpose of this paper to present an improvement over Choly's approach, which significantly reduces the coupling errors of the original approach. The improved method does not introduce any additional computational effort and is easy to implement. We demonstrate the effectiveness of the improved approach by carrying out a comparative study of bulk Al. Furthermore, we apply the new method to compute the Peierls stress of an edge dislocation in Al. The computation of Peierls stress in Al represents a difficult task because of its extremely low value. Numerical uncertainties arising from the application of boundary conditions, interatomic potentials and interpretation of the results could be comparable to the value of the Peierls stress itself. Hence, there have been large discrepancies in the theoretical/computational estimates of the Peierls stress in Al. On the experimental side, the situation is not better—the two orders of magnitude discrepancy between the Peierls stress estimated from internal friction measurements and that from mechanical testing has been tantalizing for decades [21,22]. Since the present method contains an accurate description of the dislocation core via DFT along with a reliable long-range elastic field provided by EAM, one would expect that it will give a more reliable estimate of the Peierls stress compared with previous studies.

The paper is organized as follows. In section 2, we describe the original and improved methods. In section 3, we compare the results for bulk Al using the new approach with those of the original approach and demonstrate the improved coupling across the boundary. In section 4, we present results for the dislocation core properties, including the Peierls stress for an edge dislocation in Al using the improved method. A short summary is given in section 5.

2. Method and improvement

Following the earlier work of Choly *et al* [9], the total energy of the entire system can be expressed as

$$E[\mathrm{I}+\mathrm{II}] = E_{\mathrm{DFT}}[\mathrm{I}] + E_{\mathrm{EAM}}[\mathrm{II}] + E^{\mathrm{int}}[\mathrm{I},\mathrm{II}], \tag{1}$$

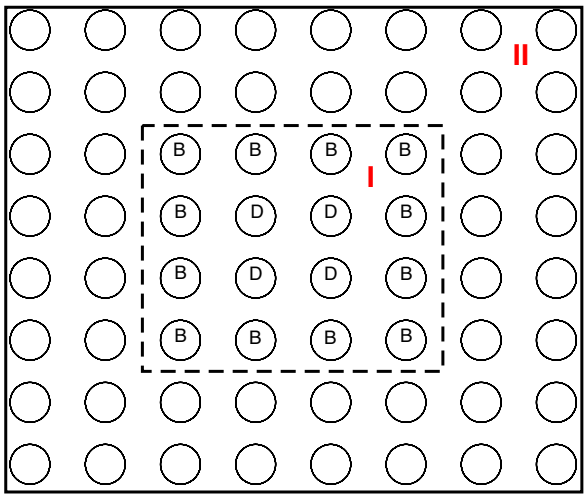

Figure 1. Schematic of the division of the system in the present multiscale approach. The entire system is divided into regions I and II. The atoms marked by 'B' denote the boundary DFT atoms upon which the force correction is applied. The atoms marked by 'D' denote inner DFT atoms or defect core atoms (see text for details).

where I refers to the small region where detailed physics are relevant and II refers to the rest of the system (figure 1). $E_{\mathrm{DFT}}[\mathrm{I}]$ is the energy of region I in the absence of region II obtained by DFT cluster calculations, $E_{\mathrm{EAM}}[\mathrm{II}]$ is the energy of region II obtained from EAM calculations in the absence of region I (i.e. void calculations) and $E^{\mathrm{int}}[\mathrm{I}, \mathrm{II}]$ represents a formal interaction energy added to give the correct total energy of the entire system. The crux of a multiscale modelling lies in the determination of $E^{\mathrm{int}}[\mathrm{I}, \mathrm{II}]$. Different choices made for the calculation of $E^{\mathrm{int}}[\mathrm{I}, \mathrm{II}]$ may result in distinct coupling methods. A similar energy expression of equation (1) had been proposed by others [23].

The interaction energy between the subsystems I and II can be written formally as

$$E^{\mathrm{int}}[\mathrm{I}, \mathrm{II}] \equiv E[\mathrm{I} + \mathrm{II}] - E[\mathrm{I}] - E[\mathrm{II}]. \tag{2}$$

In the present approach, the interaction energy is calculated by using the classical EAM potential, i.e.

$$E^{\mathrm{int}}[\mathrm{I}, \mathrm{II}] = E_{\mathrm{EAM}}[\mathrm{I} + \mathrm{II}] - E_{\mathrm{EAM}}[\mathrm{I}] - E_{\mathrm{EAM}}[\mathrm{II}]. \tag{3}$$

This of course represents an approximation to E^{int} which stipulates that the interaction energy be calculated *only* at the EAM level, the same as $E_{\mathrm{EAM}}[\mathrm{II}]$. This is a reasonable approximation because most of the atoms in a typical system are in region II and thus are described by EAM. Although more sophisticated methods, such as orbital-free DFT, could be used to calculate E^{int}, the ensuing computational effort would be much greater [9]. In other words, the present approach represents a reasonable compromise between accuracy and computational time.

This choice of the interaction energy results in a total energy of

$$E[\boldsymbol{R}^{\mathrm{tot}}] = E_{\mathrm{EAM}}[\boldsymbol{R}^{\mathrm{tot}}] - E_{\mathrm{EAM}}[\boldsymbol{R}^{\mathrm{I}}] + \min_{\{\rho^{\mathrm{I}}\}} E_{\mathrm{DFT}}[\rho^{\mathrm{I}}, \boldsymbol{R}^{\mathrm{I}}] \tag{4}$$

for a given ionic configuration $\boldsymbol{R}^{\mathrm{tot}} \equiv \boldsymbol{R}^{\mathrm{I}} \cup \boldsymbol{R}^{\mathrm{II}}$ ($\boldsymbol{R}^{\mathrm{I}}$ and $\boldsymbol{R}^{\mathrm{II}}$ are used to denote the sets of nuclear coordinates in region I and region II, respectively). The advantage of the formulation is its simplicity. It demands nothing beyond what is required for a DFT cluster calculation and two EAM calculations (one for bulk and the other for a cluster). A major practical advantage of

this approach is that, if region I contains many different atomic species while region II contains only one atom type, there is no need to have a classical potential for each species and their interactions. This results from the fact that if the various species of atoms are well within region I, then the energy contributions of these atoms cancel out in the total energy calculation (the first two terms in equation (4)). Thus, this concurrent approach is particularly useful in dealing with impurities, which is an exceedingly difficult task for classical simulations. Note that the forces on the atoms in region II are identical to the forces on these atoms if the EAM potential was used for the entire system; that is to say, as far as forces are concerned, DFT atoms act as if they were EAM atoms (this can be seen by taking the derivatives of equation (4) with respect to $\boldsymbol{R}^{\mathrm{II}}$).

On the other hand, the forces on DFT atoms in region I are

$$\boldsymbol{F}_i[\mathrm{I}] = -\frac{\partial E[\mathrm{I}+\mathrm{II}]}{\partial \boldsymbol{R}_i^{\mathrm{I}}} = \boldsymbol{F}_i^{\mathrm{EAM}}[\mathrm{I}+\mathrm{II}] - \boldsymbol{F}_i^{\mathrm{EAM}}[\mathrm{I}] + \boldsymbol{F}_i^{\mathrm{DFT}}[\mathrm{I}]. \tag{5}$$

If the cutoff length of the EAM potential is r_{c}, then those atoms in region I whose distance from the boundary is larger than r_{c} will experience a force entirely from $\boldsymbol{F}_i^{\mathrm{DFT}}[\mathrm{I}]$. Although these DFT atoms do not feel the presence of the EAM atoms, there are still errors in the force and position of these atoms due to the presence of the fictitious surface inherent in the cluster calculations of region I. On the other hand, the force on the DFT atoms that are within the distance r_{c} from the boundary has contributions both from $\boldsymbol{F}_i^{\mathrm{DFT}}[\mathrm{I}]$ and $\boldsymbol{F}_i^{\mathrm{EAM}}[\mathrm{I}+\mathrm{II}] - \boldsymbol{F}_i^{\mathrm{EAM}}[\mathrm{I}]$. Thus, the errors in the force on these DFT atoms are due to (1) the force mismatch between the DFT and EAM calculations and (2) the fictitious surface effects. It has been demonstrated [9] that the maximum and average force errors on the DFT atoms are 0.45 eV Å^{-1} and 0.33 eV Å^{-1}, respectively, in Al. The corresponding errors on the atomic positions are 0.12 Å and 0.07 Å, respectively.

In order to improve the coupling between regions I and II, we propose the following simple correction to the original approach. A third region, referred to as the boundary region, is introduced, as shown in figure 1, which consists of several layers of DFT boundary (B) atoms next to the DFT/EAM boundary. As shown below, although the boundary DFT atoms are included in the DFT cluster calculations of $E_{\mathrm{DFT}}[\mathrm{I}]$, their positions are actually determined by the EAM *bulk force* calculations. Namely, the atomic positions of the boundary atoms do not suffer from the fictitious surface effects, and they serve as a buffer to protect the inner DFT atoms from being exposed to the fictitious surface at the boundary. These inner DFT atoms are of greater interest to a given problem. For example, they could be the core of lattice defects (such as crack tip, dislocation core, grain boundary or interface), chemical impurities and active site or reaction centre, which largely determine the properties of materials. The accurate treatment of these inner DFT atoms is the focal point of the present multiscale method. More specifically, the force on the boundary DFT atoms is corrected with the term

$$\boldsymbol{F}_i^{\mathrm{corr}}[\mathrm{B}] = -\boldsymbol{F}_i^{\mathrm{DFT}}[\mathrm{B}] + \boldsymbol{F}_i^{\mathrm{EAM}}[\mathrm{B}], \tag{6}$$

so that the force on the boundary atoms is identical to that derived from the EAM calculations for the entire bulk system (I+II):

$$\boldsymbol{F}_i[\mathrm{B}] = \boldsymbol{F}_{i,\mathrm{B}}^{\mathrm{EAM}}[\mathrm{I}+\mathrm{II}]. \tag{7}$$

Since EAM gives satisfactory results for bulk properties (typically EAM potentials are fitted to reproduce bulk properties), the force on these boundary DFT atoms should be rather accurate provided that they are sufficiently far away from the defect centre. On the other hand, the force on the inner DFT atoms is determined according to equation (5), as in the original approach. Consequently, the force due to the presence of the fictitious surface is eliminated

on the boundary DFT atoms, thus protecting the inner DFT atoms from the fictitious surface. The total energy in the revised coupling scheme needs to be corrected accordingly

$$\tilde{E}[\mathrm{I}+\mathrm{II}] = E[\mathrm{I}+\mathrm{II}] - \sum_{i}^{(B)} \boldsymbol{F}_i^{\mathrm{corr}}[\mathrm{B}] \cdot \boldsymbol{u}_i[\mathrm{B}], \tag{8}$$

where $\boldsymbol{u}_i[\mathrm{B}]$ is the displacement of the ith boundary atom at each relaxation step. The sum is over all boundary atoms (B). It is clear from equation (8) that the force on region II atoms and inner DFT atoms is not affected by the correction. This energy correction is similar to that of the ghost force in the quasicontinuum approach and it represents the work done by the correction force [8]. The energy correction is not part of E^{int}. As will be shown in section 3, this simple correction can significantly reduce the force errors on both DFT and EAM atoms, with no additional computational effort.

The equilibrium structure of the entire system is obtained by minimizing the total energy in equation (8) with respect to all degrees of freedom. Because the time required to evaluate $E_{\mathrm{DFT}}[\mathrm{I}]$ is considerably more than that required to compute the EAM energetics, an alternate relaxation scheme turns out to be rather efficient. The total system can be relaxed using the conjugate gradient approach on the inner DFT atoms alone, while fully relaxing the EAM atoms in region II and the boundary atoms. Following Choly *et al*, an auxiliary energy function that only depends on the inner DFT positions can be defined as

$$E'[\boldsymbol{R}^{\mathrm{I}}] \equiv \min_{\{\boldsymbol{R}^{\mathrm{II}},\mathrm{B}\}} \tilde{E}[\boldsymbol{R}^{\mathrm{tot}}]. \tag{9}$$

The significance of E' is that its gradient with respect to $\boldsymbol{R}_i^{\mathrm{I}}$ can be easily evaluated:

$$\begin{aligned} \frac{\partial E'}{\partial \boldsymbol{R}_i^{\mathrm{I}}} &= \frac{\partial \tilde{E}[\boldsymbol{R}^{\mathrm{tot}}]}{\partial \boldsymbol{R}_i^{\mathrm{I}}} + \sum_j \frac{\partial \tilde{E}[\boldsymbol{R}^{\mathrm{tot}}]}{\partial \boldsymbol{R}_j^{\mathrm{II}}} \frac{\partial \boldsymbol{R}_{j,\mathrm{min}}^{\mathrm{II}}}{\partial \boldsymbol{R}_i^{\mathrm{I}}} \\ &= \frac{\partial \tilde{E}[\boldsymbol{R}^{\mathrm{tot}}]}{\partial \boldsymbol{R}_i^{\mathrm{I}}}, \end{aligned} \tag{10}$$

where the second term on the right-hand side of the first equation vanishes because all derivatives are evaluated at the minimum of $\tilde{E}[\boldsymbol{R}^{\mathrm{tot}}]$ with respect to $\boldsymbol{R}^{\mathrm{II}}$. The introduction of E' allows for the following relaxation algorithm. (i) Minimize $\tilde{E}[\boldsymbol{R}^{\mathrm{tot}}]$ with respect to $\boldsymbol{R}^{\mathrm{II}}$ and the boundary DFT atoms while holding the inner DFT atoms fixed. This only involves the EAM calculations. (ii) Calculate $\min_{\{\rho^{\mathrm{I}}\}} E_{\mathrm{DFT}}[\rho^{\mathrm{I}}; \boldsymbol{R}^{\mathrm{I}}]$ and $E_{\mathrm{EAM}}[\boldsymbol{R}^{\mathrm{I}}]$ and the forces on the inner DFT atoms. (iii) Perform one step of a gradient-based minimization of E' on the inner DFT atoms. (iv) Repeat the process until the entire system is relaxed. In this way, the number of DFT calculations is greatly reduced, albeit at the expense of more EAM calculations. The total number of DFT energy calculations for the relaxation of an entire system is about the same as that required for DFT calculations for the relaxation of region I alone.

3. Test of the improved method

In this section we compare the improved approach with the original one for the case of bulk Al. The system consists of $6 \times 6 \times 6$ cubic unit cells (4 atoms per cell) of crystalline fcc Al. Region I comprises the innermost 108 ($3 \times 3 \times 3$) atoms, and all other atoms are in region II. The separation in two regions is shown *schematically* in figure 1, where region I, within the dashed box, consists both of inner DFT atoms (denoted by 'D') and boundary DFT atoms (denoted by 'B'). The first shell of DFT atoms is selected as boundary atoms. For each relaxation step, a DFT cluster calculation is performed for region I whereas two separated EAM calculations

Table 1. Comparison of the maximum displacements from the perfect lattice positions for atoms in region I and region II, without and with the force correction on the boundary atoms. We also list the average displacements for atoms in region I ($\Delta u^{\mathrm{I}}_{\mathrm{av}}$) and region II ($\Delta u^{\mathrm{II}}_{\mathrm{av}}$) without and with the force correction.

	Without correction (Å)	Correction (Å)
B	0.07	0.0014
D	0.05	0.003
($\Delta u^{\mathrm{I}}_{\mathrm{av}}$)	0.03	0.0007
II	0.005	0.002
($\Delta u^{\mathrm{II}}_{\mathrm{av}}$)	0.007	0.0003

are carried out, one for the entire system (I+II) and the other solely for region I. Note that the first EAM calculation employs the periodic boundary conditions, while the second EAM calculation is non-periodic (cluster calculation). For the DFT cluster calculation, we employed the plane-wave pseudopotential VASP package [24] for a cluster with a 8 Å vacuum along the $\pm x$, $\pm y$ and $\pm z$ directions. The energy cutoff for Al is 129 eV. Only one k-point, Γ point, is used in the calculation.

The system was initially arranged in the perfect fcc lattice configuration and was then allowed to relax. Because the EAM potential used in the calculations [25] gives a lattice constant of 3.986 Å, which is slightly smaller than the corresponding DFT value of 3.990 Å, we have scaled the EAM potential so that the lattice constant from the EAM potential exactly matches the DFT value. Obviously, if the coupling between region I and region II works perfectly, the entire system would simply behave like ideal bulk Al, i.e. the system will not relax at all because the force on all atoms vanishes. On the other hand, any non-zero displacements from the initial equilibrium positions are indications of coupling errors. In table 1, we present the maximum relaxation displacements from the perfect lattice positions for both the boundary and the inner DFT atoms in region I, for the EAM atoms in region II, as well as the corresponding average value. For the boundary DFT atoms in region I and the EAM atoms in region II, the maximum displacements are reduced by more than one order of magnitude with the improved coupling method. The maximum displacements on the inner DFT atoms and the average atomic displacements in both regions are also significantly decreased. The displacements on the inner DFT atoms can be further reduced if more layers of boundary atoms are included. This however requires region I be large enough so that the inner DFT atoms are well separated from the boundary. Nevertheless, the improved coupling method allows a systematic reduction of coupling errors at a reasonable computational expense. The detailed comparison of atomic displacements in region I before and after the force correction is shown in figure 2.

4. Core properties of an edge dislocation

In this section we apply the improved coupling method to study the core structure and mobility of an edge dislocation in Al. Dislocations are a good test for multiscale approaches because their properties depend both on the atomistic details at the core and the long-range elastic strain field. More importantly, there is a wide range of conflicting experimental and theoretical results on the Peierls stress of dislocations in Al. The Peierls stress is defined as the minimum stress required to move a straight dislocation irreversibly on its glide plane [27, 28]. Theoretical values range from $10^{-5}\,\mu$ to $10^{-4}\,\mu$ for an edge dislocation, and experimental measurements span from $2.7 \times 10^{-5}\,\mu$ to $10^{-3}\,\mu$, where μ is the shear modulus of Al. In the present paper,

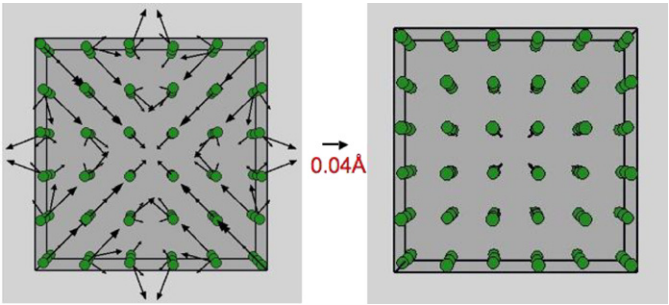

Figure 2. Displacement vectors of DFT atoms in region I without (left) and with (right) the force correction on the boundary atoms. The length of the arrow represents the magnitude of the displacement vector. The same scale is used in both figures.

the [1 1 0] shear modulus μ is about 26 GPa, obtained from the scaled EAM calculations; the corresponding DFT value is 27 GPa. The discrepancies in Peierls stress have led to various suggestions, such as the existence of a multiple core structures [26] or the interaction of vacancies with the dislocation core [29]. Therefore, it is of scientific interest to revisit the problem by multiscale modelling.

The edge dislocation with a Burgers vector $\frac{a}{2}[1\,1\,0]$ in Al ($a = 3.990$ Å) is studied in this paper. The dimensions of the entire system are 237 Å × 37 Å × 4.86 Å and those of region I are 30 Å × 15 Å × 4.86 Å. The dislocation line is along the $[\bar{1}\,1\,2]$ (z) direction and the glide direction is along the [1 1 0] (x) direction; the normal direction of the glide plane is $[1\,\bar{1}\,1]$. There are 126 DFT atoms in region I and 2748 EAM atoms in region II. One layer of DFT atoms in region I which are adjacent to EAM atoms in region II is chosen as boundary atoms. All atoms are initially displaced according to the anisotropic elastic solution of the dislocation. The boundaries along the x and y axes are held fixed to the elastic solution values during the relaxation process. Periodic boundary conditions are applied along the z direction to simulate a straight dislocation. The DFT calculations for region I are performed with a cluster of a 8 Å vacuum along both the $\pm x$ and $\pm y$ directions. The same energy cutoff of 129 eV is used. We find that 8 k points along the one-dimensional Brillouin zone are adequate for good convergence.

The dislocation core structure is summarized in figure 3. The top panel shows the relative atomic displacement across the glide plane along the x (solid line) and z (dashed line) directions. The x (z) components correspond to the edge (screw) components of the displacement field. The corresponding dislocation density (the derivative of the relative displacement with respect to x) is presented in the lower panel. The double-peak in the dislocation density plot suggests that the dislocation is dissociated into two Shockley partials whose positions are represented by the peaks. The partial separation distance is 5.9 Å, and the corresponding experimental measurement is about 5.5 Å [30]. The dislocation core width, which is defined as the atomic distance over which the x-relative displacement changes from $\frac{1}{4}b$ to $\frac{3}{4}b$, is 5.5 Å.

Because of its extremely low value, the theoretical determination of the Peierls stress in fcc metals has been challenging. The computational errors arising from the inaccuracy of the interatomic potentials, the deficiencies of continuum-based models and the improper use of boundary conditions [31] can easily reach or exceed the magnitude of the Peierls stress itself. Similarly, experimental measurement of the Peierls stress in Al has not been easy, evidenced by the two orders of magnitude of uncertainty in the results, from $2.7 \times 10^{-5}\,\mu$ to about $10^{-3}\,\mu$. To determine the Peierls stress with the present method, we apply periodic boundary conditions along both the x and z directions. Note that this is different from the core structure calculations

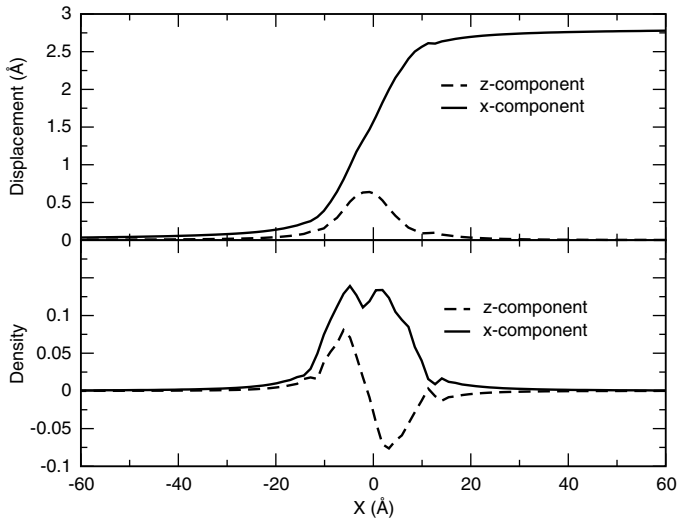

Figure 3. Top panel: the x component (solid line) and the z component (dashed line) of the relative atomic displacement as a function of x. Bottom panel: the x component (solid line) and the z component (dashed line) of the Burgers vector density as a function of the x coordinate. The double-peak structure in the density plot illustrates the dislocation dissociation into partials.

where the fixed boundary conditions were applied in the x direction. The advantage of using the periodic boundary conditions along the x direction is that the Peach–Koehler forces acting on any of the dislocations arising from their periodic images cancel identically due to the translational symmetry in x, whereas the fixed boundary conditions introduce fictitious forces from the boundary walls. In the simulation, we gradually increase the external force on the top-layer atoms along the x direction while holding the bottom-layer atoms fixed and relax the rest of the system using the conjugate gradient method described above. The applied external force on each atom is given by the desired applied shear stress multiplied by the area per atom. The centre of the dislocation is determined from the x position where the screw component of the dislocation density changes sign. We find that the centre of dislocation starts moving at the shear stress of $2.5 \times 10^{-3}\ \mu$, and the centre displacement reaches about one Burgers vector ($\sim$2.86 Å) under the shear stress of $7.5 \times 10^{-3}\ \mu$. According to the definition of Peierls stress introduced earlier, we estimate the Peierls stress to be $7.5 \times 10^{-3}\ \mu$. This result is close to the experimental value of $8 \times 10^{-3}\ \mu$ from Bujard and coworkers [22, 32]. A similar result was obtained by applying the shear stress simultaneously on both the top and bottom layers. It should be noted that the present calculations of Peierls stress represent a preliminary result, and further studies by other *ab initio*-based multiscale methods, such as in [19], are needed to ascertain the precise value of the Peierls stress.

For comparison, we have also performed EAM calculations for the entire system. The Peierls stress thus obtained is about $4.5 \times 10^{-4}\ \mu$, which is one order of magnitude smaller than the corresponding value derived from the present multiscale method. Moreover, the dislocation core width is about three times larger than that from the multiscale simulations. Therefore the lower value of the Peierls stress received from EAM simulation is consistent with the fact that the Peierls stress is smaller for a wider dislocation.

Finally, we calculate the Peierls stress by following the method introduced by Fang and Wang *et al* [33], which uses fixed boundary conditions along the x direction. In Wang's

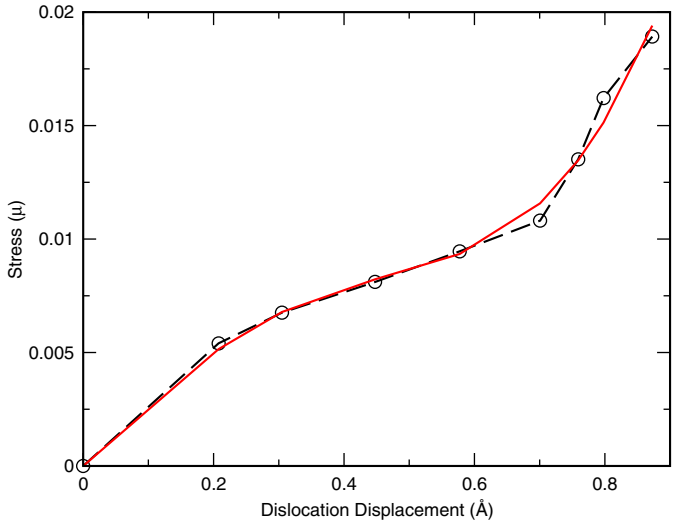

Figure 4. Applied shear stress as a function of the dislocation translation (open circles). The solid curve is the least-square fit of the simulation data to equation (11) of Wang *et al* 's method, which yields a Peierls stress of about 0.036 μ. The dashed curve is a guide to the eye.

approach, the applied shear stress, τ, as a function of the dislocation translation, u, is written as

$$\tau(u) = Ku + \tau_1 \sin\left(\frac{2\pi u}{d}\right) + \tau_2 \sin\left(\frac{4\pi u}{d}\right), \tag{11}$$

where K is a constant representing the magnitude of the image force caused by the fixed boundaries, d is the period of the Peierls potential which is the Burgers vector for an edge dislocation and τ_1 and τ_2 are constants. The Peierls stress is the maximum value of the sum of the last two terms in equation (11). The results (open circles) of the applied shear stress as a function of the dislocation translation are shown in figure 4. The solid curve in the figure, which is a least-square fit of the data to equation (11), yields a Peierls stress of 0.036μ, which is much greater than the value of $7.5\times10^{-3}\mu$ obtained from the multiscale approach, suggesting that equation (11) may not be generally applicable.

5. Summary

In conclusion, we have presented an improved coupling scheme for the multiscale modelling approach of Choly *et al* which concurrently couples DFT-based quantum mechanical calculations with empirical EAM simulations for metals. Within this scheme, the force on the DFT/EAM boundary atoms is determined from the EAM *bulk* calculations rather than from the combined DFT/EAM *cluster* calculations proposed in the original approach. In this way, the fictitious surface effects on the inner DFT atoms have been largely removed. The improved scheme reduces the coupling errors on the boundary DFT atoms and the EAM atoms by more than one order of magnitude for bulk Al, compared with the original approach. We have applied the improved method to study the core properties of an edge dislocation in Al. The Peierls stress of the dislocation is determined to be $7.5 \times 10^{-3}\,\mu$ or 195 MPa. It should be noted that the present estimate of Peierls stress needs to be further corroborated by other *ab initio*-based multiscale approaches or experiments.

Acknowledgments

The authors wish to thank Tim Kaxiras, Ellad Tadmor and Vasily Bulatov for helpful discussions. GL acknowledges the support from the Research Corporation and ACS Petroleum Research Fund. NK acknowledges the support from the US Army under Grant No W911NF-04-1-0058.

References

[1] Lu G and Kaxiras E 2005 *Handbook of Theoretical and Computational Nanotechnology* ed M Rieth and W Schommers (Stevenson Ranch, CA: American Scientific Publishers) chapter 22 and references therein
[2] Lu G, Kioussis N, Bulatov V V and Kaxiras E 2000 *Phys. Rev.* B **62** 3099
[3] Tadmor E B, Ortiz M and Phillips R 1996 *Phil. Mag.* A **73** 1529
[4] Gao J 1996 *Rev. Comput. Chem.* **7** 119
[5] Broughton J, Abraham F, Bernstein N and Kaxiras E 1999 *Phys. Rev.* B **60** 2391
[6] Bernstein N and Hess D 2001 *Mater. Res. Soc. Symp. Proc.* **653** Z2.7.1
[7] Lidorikis E, Bachlechner M, Kalia R K, Nakano A, Vashishta P and Voyiadjis G Z 2001 *Phys. Rev. Lett.* **87** 086104
[8] Shenoy V B, Miller R, Tadmor E B, Rodney D, Phillips R and Ortiz M 1999 *J. Mech. Phys. Solids* **47** 611
[9] Choly N, Lu G, W E and Kaxiras E 2005 *Phys. Rev.* B **71** 094101
[10] Shilkrot L E, Curtin W A and Miller R E 2002 *J. Mech. Phys. Solids* **50**
[11] Lu G, Tadmor E B and Kaxiras E 2006 *Phys. Rev.* B **73** 024108
[12] W E and Engquist B 2003 *Commun. Math. Sci.* **1** 87
[13] Govind N, Wang Y A and Carter E A 1999 *J. Chem. Phys.* **110** 7677
[14] Tadmor E B, Smith G S, Bernstein N and Kaxiras E 1999 *Phys. Rev.* B **59** 235
[15] Tadmor E B, Waghmare U V, Smith G S and Kaxiras E 2002 *Acta Mater.* **50** 2989
[16] W E and Huang Z 2001 *Phys. Rev. Lett.* **87** 135501
[17] Hayes R L, Ho G S, Ortiz M and Carter E A 2006 *Phil. Mag.* **86** 2343
[18] Rudd R E and Broughton J Q 1998 *Phys. Rev.* B **58** R5893
[19] Woodward C and Rao S I 2002 *Phys. Rev. Lett.* **88** 216402
[20] Daw M S and Baskes M I 1984 *Phys. Rev.* B **29** 6443
[21] Fantozzi G, Esnouf C, Benoit W and Ritchie I G 1982 *Prog. Mater. Sci.* **27** 311
[22] Nabarro F R N 1997 *Phil. Mag.* A **75** 703
[23] Elchler U, Kolmel C M and Sauer J 1996 *J. Comput. Chem.* **18** 463
[24] Kresse G and Furthmüller J 1996 *Phys. Rev.* B **54** 11169
[25] Jacobsen K W, Norskov J K and Puska M J 1987 *Phys. Rev.* B **35** 7423
[26] Srinivasan S G, Liao X Z, Baskes M I, McCabe R J, Zhao Y H and Zhu Y T 2005 *Phys. Rev. Lett.* **94** 125502
[27] Anglade P, Jomard G, Robert G and Zerah G 2005 *J. Phys. Condens. Matter* **17** 2003
[28] Moriarty J, Belak J, Rudd R, Soderlind P, Streitz F and Yang L 2002 *J. Phys.: Condens. Matter* **14** 2825
[29] Lauzier J, Hillairet J, Vieux-Champagne A and Benoit W 1989 *J. Phys.: Condens. Matter* **1** 9273
Lauzier J, Hillairet J, Gremaud G and Benoit W 1990 *J. Phys.: Condens. Matter* **2** 9247
[30] Mills M and Stadelmann P 1989 *Phil. Mag.* A **60** 355
[31] Olmsted D L, Hardikar K Y and Phillips R 2001 *Modelling Simul. Mater. Sci. Eng.* **9** 215
[32] Bujard M, Gremaud G and Benoit W 1987 *J. Appl. Phys.* **62** 3173
[33] Fang Q F and Wang R 2000 *Phys. Rev.* B **62** 9317